Journal of Applied Research in Water and Wastewater
E-ISSN: 2476-6283
Journal homepage: https://arww.razi.ac.ir

Scalable production of steam-activated wool carbon for highly efficient Cr(VI) adsorption

Sara Heshmatian[1*], Hooman Bakhshi[2], Shohreh Azizi[2], Itani Given Madiba[2]

[1]Department of Engineering Sciences and Physics, Buein Zahra Technical University, Buein Zahra, Iran.
[2]UNESCO-UNISA Africa Chair in Nanosciences-Nanotechnology, College of Graduate Studies, University of South Africa, Muckleneuk ridge, PO Box 392, Pretoria, South Africa.

GRAPHICAL ABSTRACT

ARTICLE INFO

Article type:
Research Article

Article history:
Received xx Month xxx
Received in revised form xx Month xxx
Accepted xx Month xxx
Available online x Month xx

Keywords:
Activated carbon
Steam activation
Chromium (VI) removal
Wool waste
Wastewater treatment

ABSTRACT

This study presents a sustainable approach for converting waste sheep wool into high-performance activated carbon for Cr(VI) removal from aqueous solutions. Chemical (NaOH) and steam activation routes were evaluated, and steam activation at 900 °C for 3 h in a rotary furnace produced the optimal material. The resulting carbon exhibited a high specific surface area (1807 m²/g), a pore volume of 1.002 cm³/g, and a well-developed micro-mesoporous structure. The optimized adsorbent achieved 99% removal of Cr(VI) from a 400 mg/L solution within 45 min. Physicochemical characterization (BET, SEM, XRD, Raman) and adsorption analysis (ICP-OES) confirmed the material's suitability for adsorption processes. Equilibrium behavior was best described by the Freundlich isotherm (R^2 = 0.976), while the Langmuir model yielded a monolayer capacity of 147 mg/g. Kinetic data closely followed the pseudo-second-order model (R^2 = 0.999), suggesting adsorption dominated by electrostatic interactions and surface complexation under acidic conditions. These findings demonstrate that wool waste can be effectively valorized as a low-cost, scalable, and efficient adsorbent for Cr(VI) remediation.

1. Introduction

Hexavalent chromium [Cr(VI)] is a highly toxic, carcinogenic, and persistent heavy metal widely detected in industrial effluents, particularly from leather tanning, electroplating, and dye manufacturing facilities. Even at trace levels, Cr(VI) poses severe environmental and public health risks due to its strong oxidative potential, high solubility, and mobility in aqueous media. Exposure is associated with oxidative stress, genotoxicity, and organ damage, and Cr(VI) is classified as a Group I carcinogen by the International Agency for Research on Cancer (IARC, 2012). Consequently, developing environmentally sustainable and cost-effective treatment technologies for Cr(VI) removal remains a critical priority in water purification and public health protection. Among available treatment strategies, adsorption using activated carbon (AC) is considered one of the most efficient methods because of its high specific surface area, rapid adsorption kinetics, operational simplicity, and potential for regeneration (Ahmed *et al*., 2023); (Jiao *et al*., 2020); (Oktavianty and Anggoro, 2024). However, conventional AC precursors such as coal, coconut shell, peat, and wood often rely on non-renewable resources, involve high production costs, and require environmentally intensive processing steps (Nasr, 2023). These drawbacks have driven increasing interest in valorizing agricultural and animal waste residues as renewable, low-cost alternatives for AC production, particularly within circular-economy frameworks (Tang *et al*., 2021); (Pina *et al*., 2018); (Gao *et al*., 2013); (Chen *et al*., 2013).

Wool waste, abundantly generated by leather, textile, and carpet industries, is an underutilized biomass with unique physicochemical characteristics. Its keratin-rich protein structure contains carbon,

*Corresponding author Email: heshmatian@bzte.ac.ir

Cite this article: S. Heshmatian, H. Bakhshi, Sh. Azizi, I. G. Madiba, Scalable production of steam-activated wool carbon for highly efficient Cr(VI) adsorption, *Journal of Applied Research in Water and Wastewater*, x (x), 202x, xx-xx. doi: https://doi.org/10.22126/arww.2026.13300.1455

nitrogen, and sulfur, providing intrinsic functional groups that can enhance adsorption, catalysis, and electrochemical performance (Pina *et al*., 2018); (Gao *et al*., 2013); (Chen *et al*., 2013). Several studies have demonstrated the potential of wool-derived activated carbons for removing dyes, heavy metals such as Pb(II), and organic pollutants from aqueous systems, highlighting the versatility of wool-based carbons as multifunctional adsorbents (Chen *et al*., 2013); (Rodríguez-Reinoso *et al*., 1985).

Despite these promising results, two major challenges restrict the industrial deployment of wool-based activated carbons. First, most reported studies remain confined to laboratory-scale synthesis, lacking process engineering considerations such as heat uniformity, controlled activation atmosphere, exhaust management, and continuous operation factors essential for practical scale-up (Nasr, 2023); (Tang *et al*., 2021). Second, activation strategies have not been systematically optimized. Few investigations provide a controlled comparison between chemical and physical activation routes under scalable conditions, particularly for maximizing porosity, surface area, and adsorption performance specifically for Cr(VI) removal (Gao *et al*., 2013); (Luo *et al*., 2023).

From a process engineering perspective, chemical activation routes, although effective at laboratory scale, pose significant limitations for industrial implementation, particularly for protein-based biomasses such as wool. Chemical activation typically requires large quantities of corrosive reagents, extensive post-activation washing, and generates secondary alkaline wastewater streams that complicate scale-up and increase environmental and economic costs. In contrast, steam activation offers a cleaner and more sustainable alternative by eliminating chemical effluents while enabling continuous operation, uniform heat transfer, and precise atmosphere control. Steam activation is particularly well suited for protein-rich wool precursors, as it avoids aggressive chemical treatments that may degrade keratin structures while enabling controlled pore development through gas-solid reactions. Despite these advantages, steam activation of wool-based precursors has received limited attention, and no prior study has demonstrated a scalable steam-activated wool-derived carbon system capable of achieving both high surface area and consistent adsorption performance. This gap underscores the need for a process-oriented investigation that integrates steam activation with an industrially relevant furnace design tailored to protein-rich waste materials. Chemical and steam activation mechanisms for biomass-derived carbons have been extensively reported, where alkali activation promotes matrix swelling and pore generation through dehydration reactions, while steam activation proceeds via controlled gasification reactions (C-H_2O) that selectively develop micro- and mesoporosity (Marsh and Rodríguez-Reinoso, 2006); (Lua and Yang, 2004); (Ioannidou and Zabaniotou, 2007); (Olivares-Marín *et al*., 2012).

Recent studies focusing on Cr(VI) removal using other biomass-derived carbons, including Acacia *falcata* leaves (Juturu *et al*., 2025), corncob-derived carbons (Nguyen *et al*., 2024); (Shakya and Agarwal, 2023), animal bone char (Hyder *et al*., 2015), and starch biochar (Zhang *et al*., 2025), have reported moderate to high adsorption capacities, highlighting the critical roles of pore architecture and surface chemistry in governing Cr(VI) adsorption performance. More recent approaches increasingly emphasize surface chemistry engineering, such as heteroatom doping and composite or modified biochar systems (Nasr, 2023); (Zuo *et al*., 2023). However, most of these studies remain limited to small static reactors and do not address scale-relevant aspects such as furnace design, gas handling, heat uniformity, and operational control required for pilot-scale translation. Accordingly, Table 1 compares selected biomass-derived carbonaceous adsorbents reported in the literature for Cr(VI) removal from aqueous solutions, emphasizing adsorption capacity and activation strategy rather than material chemistry alone.

A detailed comparative analysis of representative biomass-derived carbonaceous adsorbents reported in the literature is presented in the Results and Discussion section. The demonstration of rapid Cr(VI) removal across industrially relevant concentration ranges (400-1600 mg/L) provides practical evidence of the adsorbent's real-world applicability, addressing a performance gap commonly overlooked in laboratory-scale studies. Recent estimates indicate that more than 1.1 million tons of wool are produced globally each year, of which approximately 20-25% becomes waste during shearing, processing, and manufacturing stages (FAO, 2020); (The Woolmark Company, 2018); (Shavandi *et al*., 2017); (Barone and Schmidt, 2006). A significant portion of this waste is landfilled or incinerated, contributing to environmental burdens due to the slow biodegradation of keratin fibers and the release of sulfur-containing compounds. Converting wool waste into activated carbon therefore offers dual environmental benefits, namely diverting a substantial biomass stream from disposal and generating a high-value adsorbent for water treatment applications.

Motivated by the need for an energy-efficient, scalable, and industry-compatible activation system, particularly in wool-producing regions with abundant and low-cost natural gas, this study introduces a rotating, steam-assisted furnace designed to enable continuous mixing, uniform heat transfer, and controlled activation atmospheres. Unlike static laboratory reactors, the rotary configuration addresses common scale-up limitations such as uneven heating, limited steam-solid contact, and batch-to-batch variability. The optimized steam-activated wool carbon achieved a high specific surface area (1807 m^2/g) and demonstrated rapid Cr(VI) removal across industrially relevant concentrations (400-1600 mg/L), supporting its practical applicability and providing a pathway toward pilot-scale and industrial implementation.

Based on these gaps and opportunities, the present study aims to: (i) design and construct a pilot-scale rotary furnace capable of producing activated carbon from wool waste under controlled chemical and steam activation conditions; (ii) systematically compare the effects of NaOH chemical activation and steam physical activation on surface area, pore structure, morphology, and mechanical properties; (iii) evaluate the adsorption performance of the optimized carbon for Cr(VI) removal across a broad concentration range; and (iv) elucidate the adsorption mechanisms through isotherm modeling, kinetic analysis, and structural characterization. By integrating scalable reactor design with adsorption performance assessment, this study provides a comprehensive pathway for converting wool waste into an efficient, low-cost, and industrially viable adsorbent for wastewater treatment applications.

2. Materials and methods

2.1. Materials and reagents

Raw sheep wool obtained from local leather-processing industries was used as the carbon precursor. Analytical-grade sodium hydroxide (NaOH, Merck), hydrochloric acid (37% HCl, Merck), citric acid ($C_6H_8O_7$, Merk), potassium dichromate ($K_2Cr_2O_7$, Merk), and the non-ionic surfactant Triton X-100 (Merck) were used for chemical activation, washing, and preparation of Cr(VI) solutions, respectively. All solutions were prepared with deionized water.

2.2. Furnace setup

We developed a 7 L stainless-steel rotary furnace for carbonization and steam activation, featuring a 2 mm-thick rotating cylindrical chamber mounted on ball bearings and driven by a single-phase AC induction motor (Stream model, 0.37 kW, 3000 rpm). Rotational power is transmitted through a mechanical gear-and-chain reduction system, reducing the motor speed to approximately 30 rpm while increasing torque to ensure stable rotation under load. Fine control of the operating speed (10-20 rpm) is subsequently achieved using an electrical dimmer, allowing adjustment of the rotation rate during carbonization and activation. Heating is provided by a gas-fired radiant burner (Iran Radiator F55, 17,000-43,000 kcal h^{-1}), leveraging the availability of low-cost natural gas as an energy-efficient alternative to electricity at this scale. The burner is located inside a double-wall stainless steel insulated housing (Fig. 1). The activation process was conducted in a batch-operated rotary furnace under atmospheric pressure. Prior to steam activation, the wool precursor underwent an initial drying and carbonization stage at 600 °C. After completion of carbonization, the material was allowed to cool naturally to room temperature inside the furnace. The carbonized wool was subsequently subjected to a separate steam activation stage at 900 °C, during which steam was introduced into the rotating chamber and maintained for a fixed activation period. The total residence time during the steam activation stage was approximately 3 h. Continuous rotation ensured uniform heat transfer and homogeneous exposure of the material to the activating atmosphere. The system allows the introduction of either steam or nitrogen gas through the furnace inlet to enable physical or chemical activation, respectively. Exhaust gases were continuously removed and treated using a wet smoke-filtration unit prior to safe evacuation through a chimney. Thermal insulation was provided using a high-temperature ceramic fiber blanket, minimizing heat loss, stabilizing temperature profiles, and providing resistance to thermal shock and chemical degradation. Precise thermal control was achieved using a programmable multi-stage temperature controller, enabling accurate regulation of heating ramps and activation conditions.

For larger-scale systems, the same operational concept can be maintained by employing higher-power motors and appropriately sized gear-reduction units to preserve low-speed, high-torque rotation. Scale-up can therefore be achieved primarily through proportional increases in reactor volume, motor capacity, and gas flow rate, without altering the fundamental activation mechanism or process control strategy. This

modular design enables a straightforward transition from pilot-scale to industrial-scale operation.

This system integrates several engineering and economic advantages compared to conventional static reactors. The rotating cylindrical chamber and conical discharge outlet ensure uniform mixing of fibrous wool materials, minimizing localized overheating and promoting homogeneous thermal exposure. Continuous rotation improves contact between fibers, steam, and heat, resulting in more consistent activation. From an economic perspective, the use of natural gas significantly reduces operating costs compared to electricity-based laboratory reactors, particularly in gas-rich regions such as Iran. The modular configuration, combined with controlled nitrogen and steam inputs and robust ceramic insulation, ensures safe, reproducible operation and facilitates scale-up through larger batch sizes or parallel units. While modest in size, the system demonstrates global relevance for laboratories, R&D centers, and small manufacturers seeking low-cost, flexible, and reproducible activation processes with clear industrial adaptability.

Fig. 1. Rotary furnace system for wool activation: (a-b) 3-liter unit and (c-d) 7-liter pilot-scale unit. Rotating tank, discharge outlet, steam inlet and the double-wall insulated heater housing are identified with numbers (1) - (4) respectively.

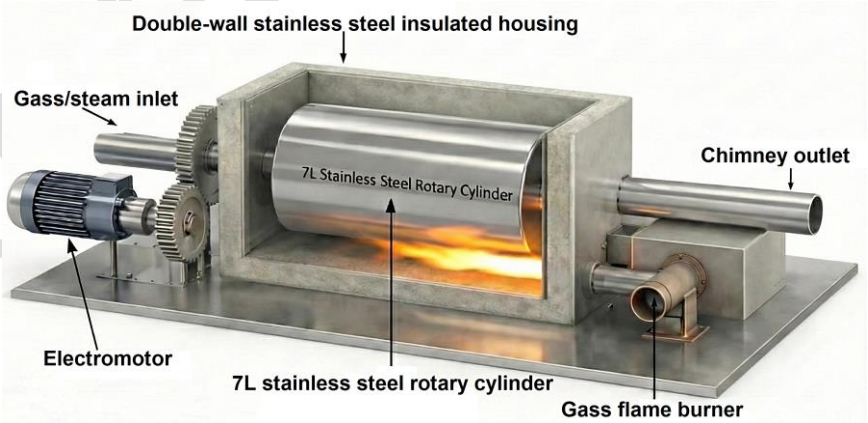

Fig. 2. Schematic illustration of the pilot-scale rotary activation furnace used for wool-derived activated carbon production.

Fig. 2 presents a schematic illustration of the rotary activation furnace developed in this study. The system consists of a horizontally oriented stainless-steel cylindrical reactor housed within a double-walled, thermally insulated chamber to minimize heat losses and maintain stable temperature profiles. The reactor is driven by an external motor to ensure continuous rotation, which promotes uniform heat transfer and homogeneous exposure of the wool precursor to the activating gases. A combined gas/steam inlet enables controlled introduction of nitrogen or steam for chemical and physical activation, respectively, while a gas-fired burner positioned beneath the reactor provides the required thermal energy. Exhaust gases exit through a dedicated outlet connected to downstream handling and filtration units, allowing safe removal of volatile by-products. This configuration enables improved temperature uniformity, enhanced gas-solid mass transfer, and superior process reproducibility compared to conventional static furnaces, thereby addressing key limitations highlighted in previous laboratory-scale activation studies.

2.3. Wool pretreatment activation procedures

Raw sheep wool was initially washed using a 2% (w/v) non-ionic surfactant solution (Triton X-100) to remove lanolin, oils, dirt, and particulate residues without altering the keratin structure. The wool was stirred at 50 °C for 20 min, followed by repeated rinsing with warm deionized water until complete removal of residual surfactant. The cleaned wool was then air-dried prior to activation. Two activation routes were investigated as described below.

All adsorption experiments were conducted using synthetic aqueous Cr(VI) solutions prepared from analytical-grade $K_2Cr_2O_7$ to ensure controlled and reproducible conditions.

2.3. Chemical activation

Pretreated wool (100 g) was immersed in 600 mL of 1 M NaOH at 85 °C for 2 h, then dried and transferred to the rotary furnace. Thermal activation was conducted at 600-800 °C for 1-3 h under a nitrogen atmosphere with continuous chamber rotation. No intermediate washing step was performed after NaOH impregnation; instead, the impregnated wool was dried and directly subjected to heat treatment, allowing residual NaOH to act as the chemical activating agent during carbonization. This approach is consistent with established alkali activation mechanisms, where NaOH promotes dehydration, matrix swelling, and pore development during thermal decomposition. After cooling under nitrogen, the activated product was collected.

2.4. Steam activation

For physical activation, 500 g of shredded wool was first carbonized at 500 °C for 1 h under nitrogen. Steam activation was subsequently performed at 700-900 °C for 1-3 h with continuous rotation at 20 rpm. Introduction of steam promoted carbon gasification according to:

$$C(s) + H_2O(g) \rightarrow CO(g) + H_2(g)\,, \qquad \text{(I)}$$

resulting in the development of micro- and mesoporous structures. To prevent oxidation, samples were removed only after cooling to below 300 °C. This gasification mechanism is characteristic of steam-activated carbons and has been widely reported for biomass precursors (Marsh and Rodríguez-Reinoso, 2006); (Olivares-Marín *et al.*, 2012).

Following both activation routes, the resulting carbons were washed with 20% HCl for 1 h to remove residual mineral species, thoroughly rinsed with deionized water until neutral pH was achieved, dried at 150 °C, and stored in airtight containers for further characterization and adsorption studies.

2.4. Preparation of Cr(VI) solutions and adsorption experiments

A 1000 mg/L Cr(VI) stock solution was prepared by dissolving potassium dichromate ($K_2Cr_2O_7$) in deionized water. Working solutions of 400, 800, 1200, and 1600 mg/L were prepared by dilution. These concentrations correspond to levels typically found in untreated effluents from electroplating, tanning, and metal-finishing industries. Batch adsorption tests were conducted by adding 0.5 g of activated carbon to 100 mL of Cr(VI) solution at 25, 50, or 75 °C for 15-45 min. All adsorption experiments were conducted at an initial solution pH of 4.0 ± 0.1, which was adjusted using dilute citric acid ($C_6H_8O_7$) prior to adsorbent addition. The pH was measured before adsorption and was not actively controlled during the adsorption process. After completion of adsorption, a slight increase in pH (typically ~0.3-0.4 pH units) was observed, likely due to surface interactions between Cr(VI) species and functional groups on the activated carbon. No buffer solutions were used in order to allow natural pH evolution during adsorption.

2.5. Characterization techniques

The structural and physicochemical characteristics of the activated carbons were systematically investigated using some analytical techniques. Nitrogen adsorption–desorption isotherms (BET/BJH method, BELSORP MINI II) were employed to determine the specific surface area, total pore volume, and pore-size distribution. Surface morphology and textural features were examined by Scanning Electron Microscopy (SEM, TESCAN MIRA3). Raman spectroscopy was utilized to assess the degree of graphitic disorder through the analysis of the D and G bands. Crystalline phases and structural ordering were characterized by X-ray diffraction (XRD). The concentration of Cr(VI) in solution before and after adsorption was quantified using Inductively Coupled Plasma Optical Emission Spectroscopy (ICP-OES). Additionally, standard ASTM methods were applied to measure the iodine number, ash content, moisture content, hardness, and bulk density of the activated carbons.

2.6. Adsorption isotherm and kinetic models

Adsorption equilibrium was modeled using Langmuir and Freundlich isotherms, while adsorption kinetics were evaluated using pseudo-first-order (PFO) and pseudo-second-order (PSO) models. The Langmuir isotherm, which assumes monolayer adsorption on homogeneous sites, is represented by Eq. 1,

$$\frac{C_e}{q_e} = \frac{1}{q_m K_L} + \frac{C_e}{q_m}\,, \qquad (1)$$

where, C_e is the equilibrium concentration of Cr(VI) in solution (mg/L), q_e is the equilibrium adsorption capacity (mg/g), q_m is theoretical maximum adsorption capacity (mg/g), and K_L is Langmuir constant related to affinity of binding sites (L/mg). The Freundlich isotherm which is suitable for heterogeneous surfaces, is expressed by,

$$\log q_e = \log K_F + \frac{1}{n}\log C_e\,, \qquad (2)$$

where K_F is the Freundlich constant indicative of adsorption capacity and n is adsorption intensity. On the other hand, kinetic behavior was evaluated using the following equation for pseudo-first-order (PFO) model,

$$\log(q_e - q_t) = \log q_e + \frac{k_1}{2.303}t\,, \qquad (3)$$

and the following equation for the pseudo-second-order (PSO) model,

$$\frac{t}{q_t} = \frac{1}{k_2\, {q_e}^2} + \frac{t}{q_e}\,. \qquad (4)$$

In Eqns. 3 and 4, q_t is the amount of Cr(VI) adsorbed at time t (mg/g), q_e is the equilibrium adsorption capacity (mg/g) and k_1 is the rate constant of PFO adsorption (1/min). All adsorption experiments (isotherm and kinetic) were conducted at ambient laboratory temperature (25 ± 2 °C), which was monitored using a calibrated glass thermometer. A standard orbital bench-top shaker (150 rpm) was used for mixing. For isotherm studies, samples were allowed to equilibrate for 24 h, which preliminary tests confirmed to be sufficient for reaching adsorption equilibrium. Kinetic experiments were performed under the same conditions, with timed sampling over a period of 0-180 min.

3. Results and discussion

To contextualize the adsorption performance of the steam-activated wool-derived carbon developed in this study, Table 1 compares its Langmuir maximum adsorption capacity and textural properties with those of representative biomass-derived carbons reported for Cr(VI) removal. Emphasis is placed on adsorption capacity (q_m) and activation strategy, as removal efficiencies alone are strongly dependent on experimental conditions. This table summarizes the activation method, Langmuir maximum adsorption capacity (q_m), specific surface area (SSA), maximum removal efficiency, and contact time where explicitly reported. Dashes indicate that the corresponding parameter was not explicitly reported in the original publication. In addition to maximum removal efficiency, Langmuir maximum adsorption capacities are included to ensure a more robust comparison.

3.1. Textural and surface properties

Nitrogen adsorption-desorption isotherms reveal distinct differences between chemically and physically activated samples. Chemically activated carbons exhibit Type I isotherms (Fig. 3a), characterized by pronounced nitrogen uptake at low relative pressure ($P/P_0 < 0.1$), indicating predominantly microporous structures. In contrast, the steam-activated sample exhibits a Type IV isotherm with an H3-type hysteresis loop (Fig. 3b), indicating the coexistence of micropores and mesopores formed during the steam-carbon gasification process. The steep uptake at low relative pressure confirms abundant microporosity, while the pronounced hysteresis at intermediate pressures ($P/P_0 \approx 0.4$-0.9) reflects capillary condensation within slit-shaped mesopores. This mixed porosity is characteristic of steam activation at elevated temperature and correlates with the substantially higher surface area and pore volume measured for this sample. BET and BJH results for chemically activated samples are listed in Table 2. Increasing activation temperature from 600 to 800 °C increases the specific surface area (SSA) from 181 to 432 m^2/g and doubles the pore volume (0.098 to 0.196 cm^3/g). The observed decrease in pore diameter with increased temperature suggests progressive development of narrower micropores. Solid-state NaOH activation (Table 2, experiments 10-12) performed poorly due to limited reagent penetration.

Table 1. Comparison of biomass-derived carbonaceous adsorbents reported in the literature for Cr(VI) removal from aqueous solutions.

Contact time (min)	Max removal (%)	SSA (m^2/g)	Langmuir q_m (mg/g)	Activation method	Material	Reference
45	99	1807	147	Steam (900°C, 3 h)	Sheep wool	This study
180	~95	472.98	114.09	H_3PO_4/OPA+ magnetization	Acacia falcata leaves	Juturu *et al.*, 2025
120-1080	91-94	-	149.21	Hydrothermal	Starch	Zhang *et al.*, 2025
5-270	~57	-	38.1	Pyrolysis (500-700 °C)	Corncob	Nguyen *et al.*, 2024
60-180	>95	520-860	~63-92	Pyrolysis (500-700 °C)	Corncob	Shakya and Agarwal, 2023
120	>90	~300	~40-65	Pyrolysis	Animal bone	Hyder *et al.*, 2015

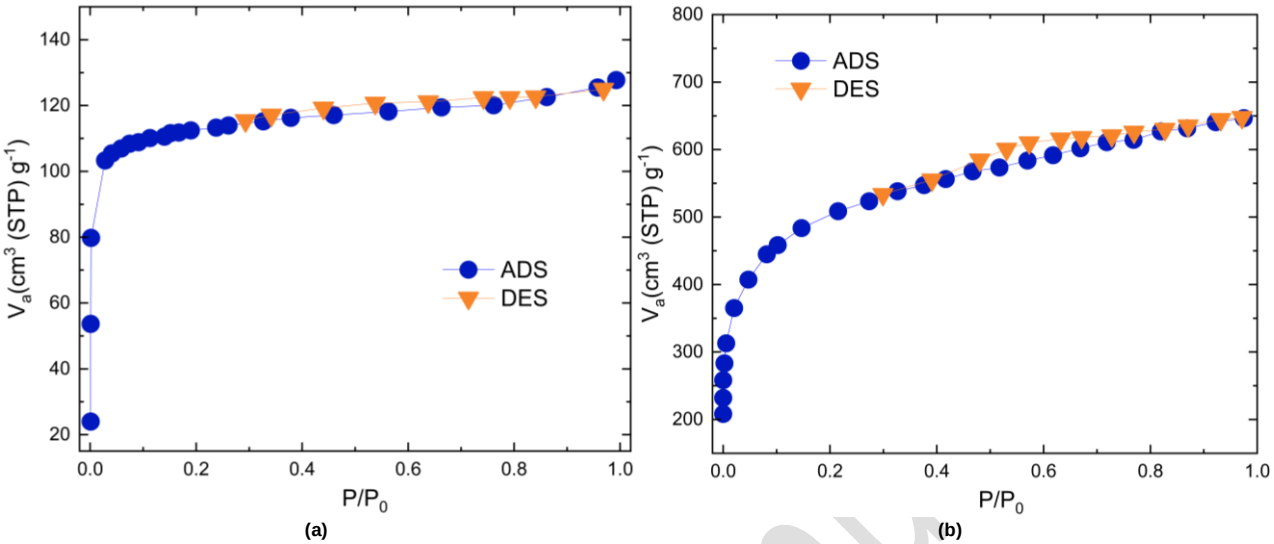

Fig. 3. N_2 adsorption-desorption isotherms: (a) chemically activated sample (NaOH-700-3h), showing microporosity; (b) steam-activated sample (Steam-900-3h), showing mixed porosity.

Steam activation produces significantly high textural properties (Table 3). Increasing the activation temperature and residence time enhances pore development, with the optimal sample (Steam-900-3h) achieving an SSA of 1807 m^2/g and a total pore volume of 1.002 cm^3/g, outperforming many biomass-derived activated carbons reported in literature. The high SSA values obtained (up to 1807 m^2/g) fall within the typical range reported for steam-activated wool-based biomasses. Also, the pore volume values fall within the expected 0.3-1.1 cm^3/g range for steam-activated biomass carbons. The pore development mechanism is governed by the steam-carbon gasification reaction of Eq. (*I*), which progressively removes carbon atoms and generates new micro- and mesopores. At lower temperatures (700-800 °C), pore evolution is less pronounced, whereas 900 °C provides optimal activation conditions. The exceptional SSA and pore volume achieved demonstrate both the effectiveness of steam activation and the advantages of the rotary furnace system. Similar trends in pore development and surface area enhancement have been reported for mechanochemically activated carbons and vacuum-pyrolyzed biomass-derived materials, where activation conditions strongly control micropore and mesopore formation (Szczęsniak *et al.*, 2020); (Rodríguez-Reinoso *et al.*, 1987); (Carrier *et al.*, 2012).

Table 2. BET analysis results for chemically activated samples.

Sample no.	Agent	Agent: precursor	Time (h)	Temp. (°C)	Pore diameter (nm)	Pore volume (cm^3/g)	SSA (m^2/g)
1	NaOH solution	1:3	3	600	2	0.098	181
2	NaOH solution	1:3	3	700	1.84	0.181	394.2
3	NaOH solution	1:3	3	800	1.8	0.196	432
4	NaOH solution	1:3	2	600	2.2	0.090	161
5	NaOH solution	1:3	2	700	2	0.125	249
6	NaOH solution	1:3	2	800	1.81	0.179	394.5
7	NaOH solution	1:3	1	800	2.2	0.176	318
8	NaOH solution	1:1	3	800	2.2	0.095	165
9	NaOH solution	1:2	3	800	2	0.166	333
10	NaOH powder	1:3	3	600	8.9	0.012	5.6
11	NaOH powder	1:3	3	700	2.4	0.045	74
12	NaOH powder	1:3	3	800	2.4	0.097	161

Table 3. BET surface area, pore volume, and pore diameter of steam-activated wool carbons at different temperatures and activation times.

Sample no.	Agent: Precursor	Time (h)	Temp. (°C)	Pore Diameter (nm)	Pore Volume (cm^3/g)	SSA (m^2/g)
13	500	3	700	2.4	0.564	939
14	500	3	800	2.4	0.297	1136
15	500	3	900	2.2	1.002	1807
16	500	2	700	1.98	0.415	836
17	500	2	800	2.6	0.306	1133
18	500	2	900	3.1	0.353	1343
19	500	1	700	2.3	0.401	731
20	500	1	800	2.5	0.606	959
21	500	1	900	2.89	0.261	1175
22	400	3	700	21	0.415	776
23	400	3	800	1.7	0.297	1023
24	400	3	900	1.7	0.457	1072

3.2. Morphology and structural analysis

The XRD pattern of the steam-activated wool-derived carbon (Fig. 4a) exhibits a broad diffraction feature centered at 2θ ≈ 24-26°, which is commonly associated with the (002) reflection of turbostratic carbon materials (PDF 75-1621). The broad and low-intensity nature of this feature indicates a predominantly amorphous carbon structure with limited short-range ordering, typical of steam-activated biomass-derived carbons, rather than well-crystallized graphite. No diffraction peaks corresponding to crystalline metal oxides or inorganic salts were detected, confirming the effective removal of mineral residues during post-activation acid washing. Raman spectra (Fig. 4b) further support this interpretation, showing the characteristic D and G bands at approximately 1350 and 1600 cm^{-1}, respectively. The ID/IG ratios (1.1-1.3) indicate a high density of structural defects and disordered carbon domains. This is consistent with the turbostratic carbon structure inferred from XRD analysis and favorable for adsorption applications.

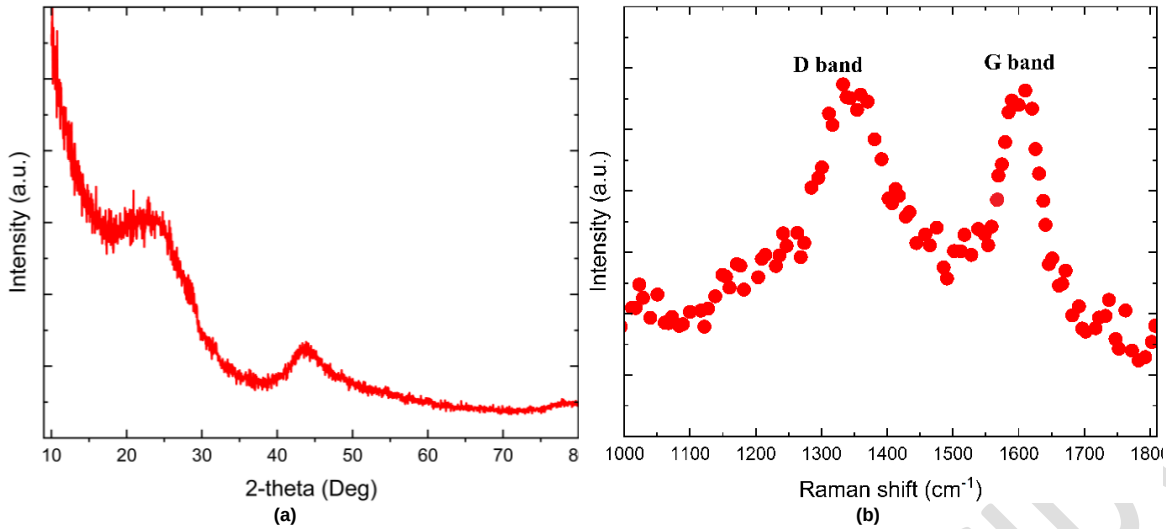

Fig. 4. (a) XRD pattern and (b) Raman spectrum of optimized steam-activated sample.

SEM images (Fig. 5) clearly illustrate the progressive morphological transformation of wool-derived carbon during activation. The high-magnification micrograph in Fig. 5a (200 nm scale) reveals a compact and relatively smooth surface characteristic of carbonized wool prior to activation. In contrast, the steam-activated samples (Figs. 5b-d) exhibit systematic development of porosity at multiple length scales. Early-stage activation (Fig. 5b, 500 nm) shows the initiation of surface roughening and small pore openings, while more advanced activation (Fig. 5c, 1 µm) displays interconnected mesoporous structures and fractured carbon domains. At the largest scale (Fig. 5d, 2 µm), pronounced macropores and widened cavities are observed, consistent with gasification-induced carbon removal during steam activation.

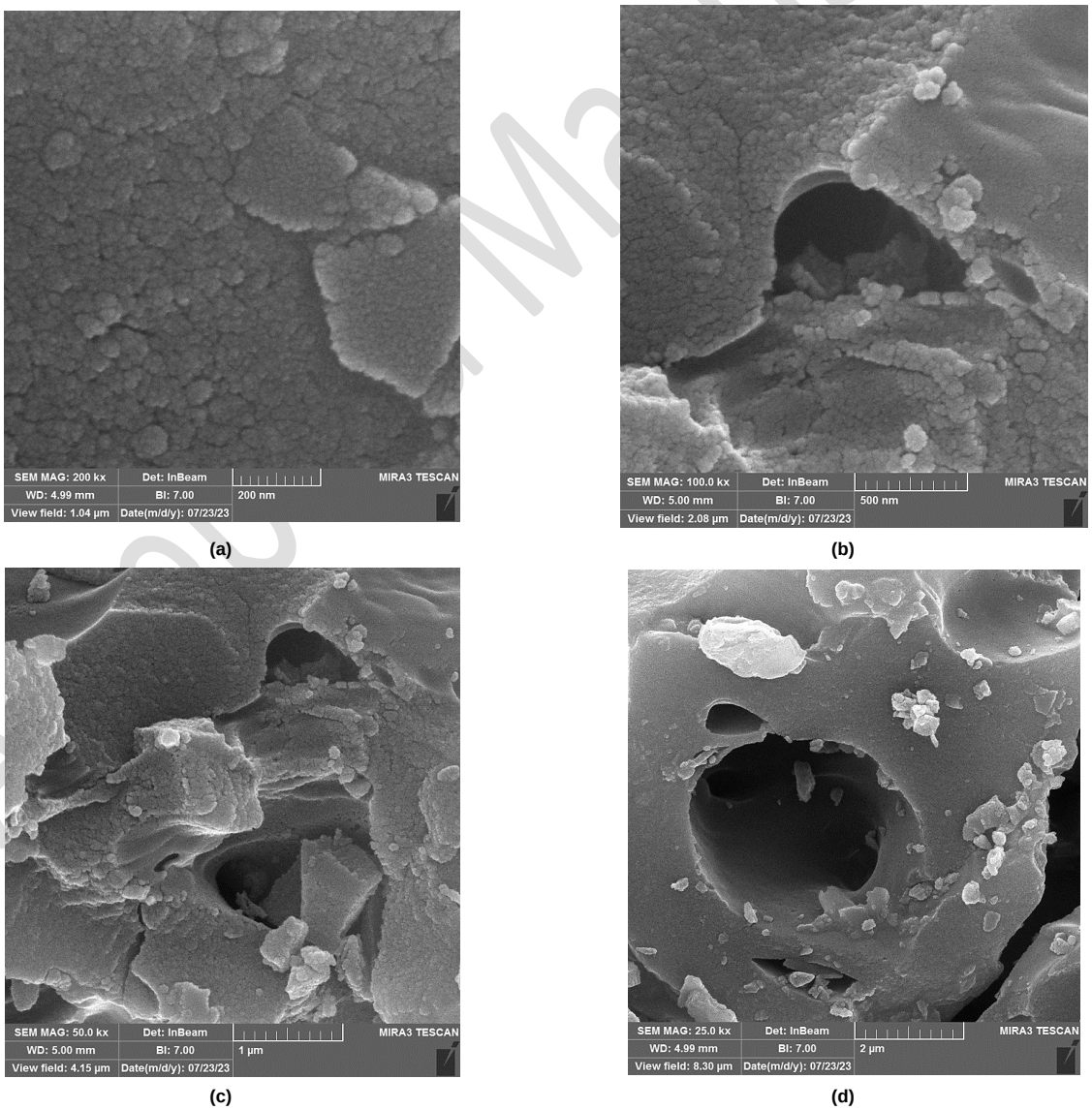

Fig. 5. SEM micrographs illustrating the hierarchical pore development in wool-derived activated carbon. (a) High-magnification image (200 nm scale) showing nanoscale granular structures on the activated surface; (b) early-stage pore opening at the sub-micron level (500 nm scale); (c) development of fractured domains and mesoporous regions (1 µm scale); and (d) emergence of widened macro-pores following high-temperature steam activation (2 µm scale).

These features confirm the hierarchical porosity generated during activation. Uniformity of pore development was verified by repeated SEM examinations of multiple independently prepared batches, demonstrating the reproducibility of the activation conditions and the consistency of the resulting material morphology. It should be noted that SEM primarily reveals surface morphology and meso- to macroporous features, while microporosity cannot be directly resolved at this scale. Accordingly, the dominant microporous character inferred from BET analyses and iodine number (1050 mg/g) complements the SEM observations. In samples exhibiting high total pore volume but comparatively moderate specific surface area, the presence of SEM-observed fissures and macroporous cavities provides a plausible structural explanation, as such larger voids contribute significantly to pore volume while contributing less to surface area.

3.3. Granulometry and mechanical stability

Granulometric analysis (Table 4) shows that approximately 50% of the activated carbon is retained on an 8-mesh sieve (2360 µm), while only 2.86% passes through an 18-mesh sieve (1000 µm). This relatively coarse distribution is advantageous for packed-bed filtration systems, where excessive fines can increase pressure drop and clogging risk.

Mechanical testing using the ball-pan hardness method resulted in values above 99%, demonstrating excellent abrasion resistance. This high mechanical stability supports the suitability of wool-derived activated carbon for continuous-flow or recirculating treatment systems. Comparable mechanical resilience has been observed for activated carbons prepared from industrial and agricultural residues, such as malt bagasse and other high-ash precursors, which are similarly targeted for robust process applications (Rodríguez *et al.*, 2016); (de Lima and Anschau, 2019).

Table 4. Granulation determination test.

Sieve number	Aperture (µm)	Mass retained (%)
0.25	6300	0.0
4	4750	2.46
6	3350	20.98
7	2810	13.21
8	2360	22.81
10	2000	14.29
12	1700	13.06
14	1400	9.80
18	1000	2.86
20	850	0.33
25	710	0.0

3.4. Chemical composition

The physicochemical characteristics of the optimized sample (Steam-900-3h) are summarized in Table 5. The iodine number, 1050 mg/g, was determined following ASTM D4607 (iodine adsorption from standard iodine solution with thiosulfate titration after equilibration), and reported as mg I_2 adsorbed per g carbon. Was used it as a proxy indicator of microporosity, complementing BET/BJH analysis which reflects a high degree of microporosity. On the other hand, the methylene blue value (145 mg/g) confirms the presence of mesopores that enhance transport of larger ions and molecules.

Table 5. Physicochemical properties of optimal activated carbon.

Property	Value	Standard
Iodine value	1050	ASTM D4607
Ash content (%)	0.3	ASTM D2866
Density (g/cm³)	0.57	ASTM D2854
Moisture (%)	3.7	ASTM D2867
Hardness (Ball-Pan)	99.2	ASTM D3802
Methylene Blue (mg/g)	145	IS 877

The ash content (0.3%) is far below critical thresholds for drinking-water-grade activated carbon, minimizing the risk of leachable inorganic impurities. The bulk density (0.57 g/cm^3) and moisture content (3.7%) align well with commercially available granular activated carbons. The combination of low ash, high surface area, and strong mechanical properties makes this material highly competitive for industrial-scale adsorption applications. The iodine and methylene blue values obtained are also consistent with those reported for acid-activated rice husk carbons used in heavy-metal removal from wastewater (Hanum *et al.*, 2017).

3.5. Adsorption performance and modeling

3.5.1. Cr(VI) adsorption performance

The optimized activated carbon exhibits rapid and highly effective Cr(VI) removal. At 25 °C and an initial concentration of 400 mg/L, removal efficiencies reach from 94% to 99% during the time interval of 15-45 minutes. At higher Cr(VI) concentrations (800-1600 mg/L), removal efficiencies remain strong (79-91%), as summarized in Table 6, though partial saturation becomes evident at the highest loadings. The consistently high removal efficiencies observed across all concentrations can be attributed in part to the low operating pH (≈4), which favors both protonation of surface functional groups and the predominance of $HCrO_4^-$ species, thereby enhancing electrostatic adsorption (see Table 6).

The operating ranges reported in this table were selected to reflect practical treatment conditions and to probe performance-limiting factors. Initial Cr(VI) concentrations of 400-1600 mg/L were chosen to represent heavily contaminated industrial effluents and to evaluate adsorbent behavior under high loading. Contact time range of 15-45 min was selected based on preliminary kinetic screening showing rapid uptake within this window, enabling assessment of short, operationally relevant treatment times. Temperatures of 25, 50, and 75 °C were included to examine the effect of temperature on adsorption efficiency and infer the adsorption thermodynamic tendency (endothermic vs exothermic). All experiments were conducted at an initial pH of 4.0 ± 0.1 to ensure consistent Cr(VI) speciation and comparability across conditions.

Table 6. Cr(VI) removal performance under various conditions (initial pH = 4.0 ± 0.1).

Exp.	Temp. (°C)	Initial concentration (mg/L)	Time (min)	Final concentration (mg/L)	Remova (%)
25	25	400	15	23.62	94
26	25	400	30	9.33	97
27	25	400	45	4.62	99
28	25	400	45	4.62	99
29	25	800	45	67.41	91
30	25	1200	45	213.56	82
31	25	1600	45	324.28	79
32	50	800	45	79.36	90
33	75	800	45	132.46	83

Elevated temperatures (50 and 75 °C) slightly reduce removal efficiency, indicating that Cr(VI) adsorption is exothermic in nature. The rapid removal rate is consistent with the high SSA, interconnected pore network, and abundant surface functional groups. It should be mentioned that, all adsorption experiments were conducted in duplicate, and the observed adsorption trends were highly reproducible across independent runs. While full statistical error bars are not presented for all datasets due to limited replicate measurements, the consistency of adsorption behavior and the high correlation coefficients (R^2) obtained from kinetic and isotherm model fittings support the reliability of the experimental results. Future work will include expanded replicate testing to enable comprehensive statistical analysis and uncertainty quantification. Also, desorption/regeneration testing was not performed in the present study. However, based on the adsorption conditions (initial pH ≈ 4) and the proposed dominant interactions (electrostatic attraction and surface complexation), regeneration is expected to be feasible using alkaline eluents and/or salt solutions.

3.5.2. Isotherm modeling

Adsorption equilibrium data were evaluated using Langmuir and Freundlich isotherms. For the Langmuir isotherm (Eq. 1), plotting C_e/q_e vs. C_e produced a linear fit with $R^2 = 0.948$, yielding a maximum monolayer adsorption capacity of $q_m = 147\ mg/g$ (Fig. 6a). This indicates that the surface possesses well-defined adsorption sites capable of uniform Cr(VI) uptake. The Freundlich model provided a slightly stronger statistical fit ($R^2 = 0.976$, Fig. 6b). The Freundlich constant n = 4.16 (1 < n < 10) confirms favorable and nonlinear multilayer adsorption. These results suggest that, although the Freundlich model fits the data more closely, the Langmuir model is important for estimating the theoretical capacity of $q_m = 147\ mg/g$ which places this material among the most effective bio-derived adsorbents reported in the literature (Ahmad *et al*., 2012); (Zhang *et al*., 2025). The combination of models indicates that Cr(VI) adsorption occurs through both monolayer binding and multilayer interactions, reflecting the material's heterogeneous surface chemistry. The suitability of Langmuir and Freundlich models for describing adsorption

on heterogeneous carbon surfaces agrees with fractal and empirical isotherm analyses reported for other activated carbons (Kano *et al*., 2000). Furthermore, the maximum capacity obtained in this study is comparable to or higher than that of pistachio-shell-derived activated carbon and starch biochar applied to dye and Cr(VI) adsorption, respectively (Foo and Hameed, 2010); (Zhang *et al.*, 2025).

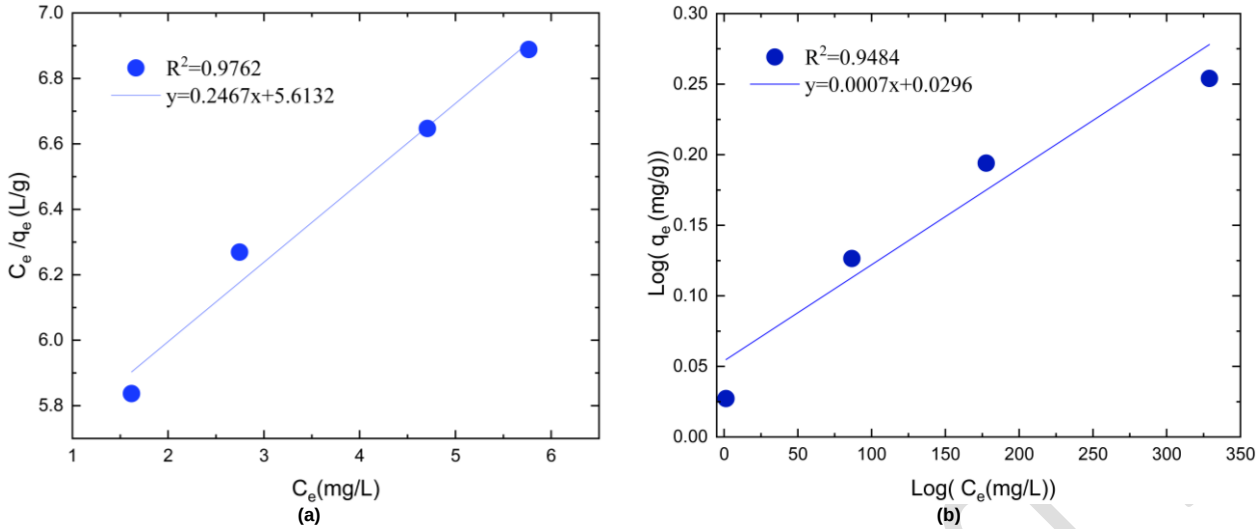

Fig. 6. Linearized adsorption isotherm models for Cr(VI) removal: (a) Langmuir plot showing C_e/q_e vs. C_e, and (b) Freundlich plot showing $Log(q_e)$ vs. $Log(C_e)$.

3.5.3. Kinetic modeling and chemisorption mechanism

Adsorption kinetics were evaluated using pseudo-first-order (PFO) and pseudo-second-order (PSO) models. From Fig. 7a, it could be observed that, the PFO model (Eq. 3) showed a strong correlation with $R^2 = 0.993$, indicating that the early adsorption stage is influenced by the availability of unoccupied sites. On the other hand, the PSO model (Eq. 4) showed the best fit with $R^2 = 0.999$, as shown in Fig. 7b. The obtained value of $q_e \approx 79\ mg/g$ is consistent with the experimentally observed adsorption capacity. This value aligns with the maximum possible Cr(VI) uptake based on the initial concentration and adsorbent dosage (400 mg/L, 100 mL, 0.5 g), and remains below the Langmuir monolayer capacity (147 mg/g). The good agreement between experimental and model-derived q_e confirms chemisorption as the dominant mechanism. Dominance of PSO kinetics has similarly been reported for dye and metal adsorption on various activated carbons, particularly when chemisorption and surface reaction steps control the overall rate (Lin and Wang, 2009). The kinetic results and high correlation with the pseudo-second-order model suggest that chemisorption plays an important role in Cr(VI) removal. The likely contributing processes include (i) electrostatic attraction between protonated functional groups on the wool-derived carbon and Cr(VI) oxyanions ($HCrO_4^-$, $Cr_2O_7^{2-}$), and (ii) Surface complexation on oxygen- and nitrogen-containing functional groups. These interactions are supported by changes in Raman spectra (Fig. 4b), which indicate modification of surface functional groups following adsorption.

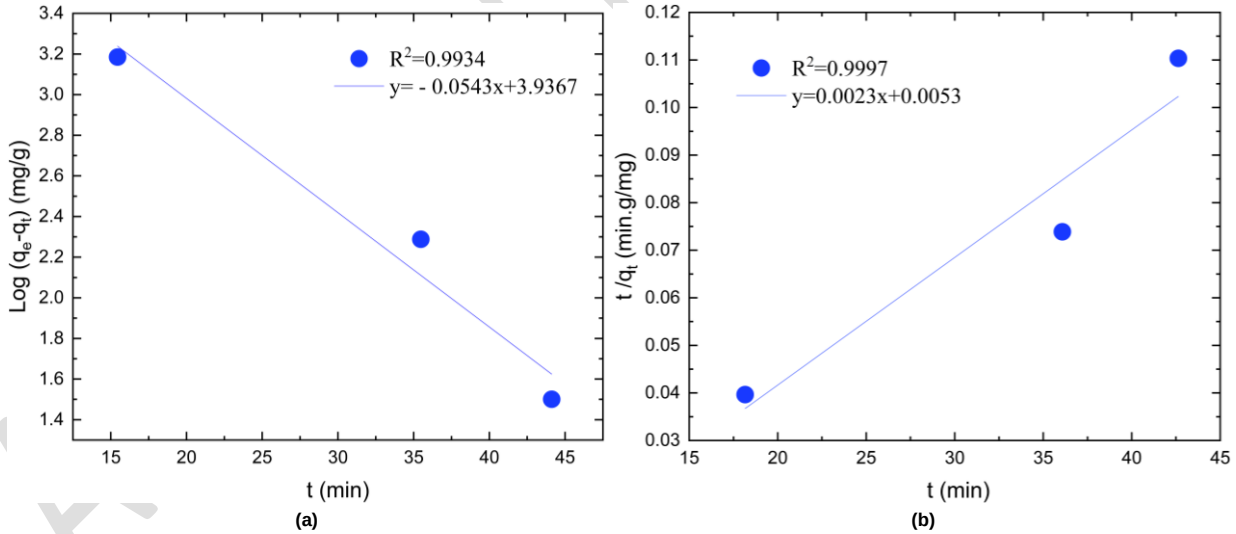

Fig. 7. Linearized kinetic models for Cr(VI) adsorption: (a) pseudo-first-order model and (b) pseudo-second-order model.

The integrated effects of rapid kinetics, strong affinity, and redox activity make the wool-derived activated carbon highly suitable for real wastewater treatment applications. These observations are consistent with broader studies on chemisorption mechanisms of heavy metals onto functionalized carbon materials, which highlight the combined roles of electrostatic attraction, redox transformation, and inner-sphere complexation (Burakov *et al*., 2018). A summary of isotherm and kinetic model parameters is presented in Table 7.

Table 7. Constants and fit quality of isotherm and kinetics models.

Model	q_e or q_m (mg/g)	k	R^2	K	$1/n$	n
Langmuir	$q_m = 147$	-	0.948	$K_L = 0.031$	-	-
Freundlich Isotherm	-	-	0.976	$K_F = 274.02$	246	4.16
Pseudo-First Order	$q_e = 79.1$	$k1 = 0.0543$	0.993	-	-	-
Pseudo-Second Order	$q_e = 79.1$	$k2 = 0.001$	0.999	-	-	-

Taken together, the adsorption performance data, modeling results, and structural characterizations provide a coherent and self-consistent description of Cr(VI) removal by the wool-derived activated carbon. The high removal efficiencies observed at acidic pH (≈4) are consistent with the predominance of $HCrO_4^-$ species in solution and the protonation of surface functional groups, which collectively enhance electrostatic attraction and surface complexation (Burakov *et al*., 2018); (Mohan *et al.*, 2006). The strong agreement between experimentally determined adsorption capacities and those predicted by the Langmuir and Freundlich isotherms, together with the excellent fit of the pseudo-

second-order kinetic model, indicates that chemisorption-controlled processes dominate Cr(VI) uptake (Ho and McKay, 1999); (Foo and Hameed, 2010).

Morphological and structural analyses further support this interpretation. SEM observations reveal a highly developed porous architecture that facilitates rapid mass transfer, while Raman spectroscopy indicates abundant defect sites and disordered carbon domains capable of interacting with oxyanion species (Ferrari and Robertson, 2000); (Tuinstra and Koenig, 1970). XRD patterns confirm the predominantly amorphous nature of the activated carbon, consistent with heterogeneous adsorption behavior inferred from isotherm modeling (Rodríguez-Reinoso, 1998). Although direct spectroscopic evidence of Cr(VI) reduction to Cr(III) is not available in the present study, the combined influence of acidic conditions, surface functional groups, and kinetic behavior suggests that redox-assisted adsorption *may contribute* alongside electrostatic attraction and surface complexation, as reported for other biomass-derived carbonaceous adsorbents (Burakov *et al*., 2018); (Valentín-Reyes *et al*., 2019). This integrated interpretation provides a robust framework for understanding Cr(VI) removal while remaining consistent with the available experimental evidence.

4. Conclusions

This study demonstrates the successful conversion of waste sheep wool into a high-performance activated carbon through a scalable, steam-assisted rotary activation process. Steam activation at 900 °C produced an adsorbent with a high specific surface area of 1807 m²/g and a well-developed micro-mesoporous structure, significantly exceeding most surface areas previously reported for wool-derived carbons. The optimized material exhibited rapid and efficient Cr(VI) removal, achieving 99% removal within 45 min from a 400 mg/L solution and a Langmuir maximum adsorption capacity of 147 mg/g, confirming its strong adsorption affinity under acidic conditions. A slight increase in solution pH after adsorption was observed consistent with proton consumption during Cr(VI) uptake and surface complexation, a behavior commonly reported for acidic Cr(VI) adsorption systems. Comparative analysis of chemical (NaOH) and physical (steam) activation revealed that steam activation offers a favorable balance between pore development, structural integrity, and scalability, while avoiding extensive post-treatment washing and chemical waste generation. Adsorption behavior was well described by the Freundlich isotherm and pseudo-second-order kinetic model, indicating heterogeneous surface interactions dominated by surface complexation and electrostatic attraction. While Cr(VI) removal was highly effective, the absence of direct Cr speciation analysis precludes definitive confirmation of reduction to Cr(III), and adsorption is therefore considered the dominant removal mechanism under the studied conditions. Importantly, the integration of a rotating, gas-fired furnace enabled uniform heat transfer, continuous mixing, and controlled activation atmospheres, addressing key limitations associated with static laboratory reactors. The demonstrated performance across industrially relevant Cr(VI) concentrations (400-1600 mg/L) highlights the practical applicability of the developed adsorbent and supports the potential for scale-up by increasing reactor volume, motor capacity, and gas flow without altering the fundamental process design. Overall, this work demonstrates that waste sheep wool can be transformed into a high-performance activated carbon through a scalable, steam-assisted rotary activation process, achieving a specific surface area of 1807 m²/g and a Langmuir adsorption capacity of 147 mg/g for Cr(VI), values that exceed most previously reported wool-derived carbons. The combination of rapid removal kinetics, stable performance across industrially relevant concentrations, and an energy-efficient, gas-fired rotary furnace design establishes a clear advancement over conventional laboratory-scale approaches. This integrated materials-process strategy represents a meaningful step toward industrial implementation of protein-based waste valorization for sustainable water treatment.

Despite the promising results, several important challenges remain. Regeneration and long-term reusability of the adsorbent were not evaluated, and adsorption tests were performed only in synthetic Cr(VI) solutions, leaving performance in real wastewater matrices uncertain. Future work should address multi-cycle regeneration, Cr(VI)/Cr(III) speciation, techno-economic assessments, continuous-flow operation, and applicability to multi-contaminant systems to fully establish the industrial feasibility of this process.

Author Contributions

Sara Heshmatian: Supervisor, conceptualization, review, writing the first draft.
Hooman Bakhshi: Investigation, analysis and experiments.
Shohreh Azizi: Conceptualization, editing and modeling.
Itani Madiba: Conceptualization, editing and modeling.

Conflict of Interest

The authors declare that there is no conflict of interest regarding the publication of this paper.

Data Availability Statement

The data presented in this study is available on request from the corresponding author.

References

Ahmad, M. *et al.* (2012) 'Effects of pyrolysis temperature on soybean stover- and peanut shell-derived biochar properties and TCE adsorption in water', *Bioresource Technology*, 118, pp. 536-544. doi: https://doi.org/10.1016/j.biortech.2012.05.042

Ahmed, A.S. *et al.* (2023) 'Carbon dioxide adsorption by a high-surface-area activated charcoal', *Journal of Composites Science*, 7(5), p.179. doi: https://doi.org/10.3390/jcs7050179

Barone, J.R., Schmidt, W.F. and Gregoire, N.T. (2006) 'Extrusion of feather keratin', *Journal of Applied Polymer Science*, 100(2), pp. 1432-1442. doi: https://doi.org/10.1002/app.23501

Carrier, M. *et al.* (2012) 'Production of char from vacuum pyrolysis of South African sugar cane bagasse and its characterization as activated carbon and biochar', *Journal of Analytical and Applied Pyrolysis*, 96, pp. 24-32. doi: https://doi.org/10.1016/j.jaap.2012.02.016

Chen, W. *et al.* (2013) 'Activated carbon powders from wool fibers', *Powder Technology*, 234, pp. 76-83. doi: https://doi.org/10.1016/j.powtec.2012.09.026

de Lima, R. C. A. and Anschau, A. (2019) 'Characterization of Activated Charcoal Obtained from Malt Bagasse', *Orbital: The Electronic Journal of Chemistry*, 11(6), pp. 374-377. doi: https://periodicos.ufms.br/index.php/orbital/article/view/15809

FAO (2020) 'World Statistical Compendium for Raw Hides and Skins, Leather and Leather Footwear 1999-2020', *Food and Agriculture Organization of the United Nations*.

Ferrari, A.C. and Robertson, J. (2000) 'Interpretation of Raman spectra of disordered and amorphous carbon', *Physical Review B*, 61(20), pp.14095-14107. doi: https://doi.org/10.1103/PhysRevB.61.14095

Foo, K.Y. and Hameed, B.H. (2010) 'Insights into the modeling of adsorption isotherm systems', *Chemical Engineering Journal*, 156(1), pp. 2-10. doi: https://doi.org/10.1016/j.cej.2009.09.013

Foo, K.Y. and Hameed, B.H. (2011) 'Preparation and characterization of activated carbon from pistachio nut shells by microwave-induced chemical activation: Application for methylene blue adsorption', *Chemical Engineering Journal*, 180, pp. 66-74. doi: 10.1016/j.biombioe.2011.04.023

Gao, Q. *et al.* (2013) 'Preparation and characterization of activated carbon from wool waste and comparison of muffle furnace and microwave heating methods', *Powder Technology*, 249, pp. 234-240. doi: https://doi.org/10.1016/j.powtec.2013.08.029

Olivares-Marín, M. *et al.* (2012) 'Preparation of activated carbon from cherry stones by physical activation in air. Influence of the chemical carbonisation with H2SO4', *Journal of Analytical and Applied Pyrolysis*, 94, pp.131-137, https://doi.org/10.1016/j.jaap.2011.11.019

Hanum, F., Bani, O. and Wirani, L.I. (2017) 'Characterization of activated carbon from rice husk by HCl activation and its application for Pb removal in Car Battery Wastewater', *IOP Conference Series: Materials Science and Engineering*, 180(1), p. 012151. doi: https://doi.org/10.1088/1757-899X/180/1/012151

Ho, Y.S. and McKay, G. (1999) 'Pseudo-second order model for sorption processes', *Process Biochemistry*, 34(5), pp. 451-465. doi: https://doi.org/10.1016/S0032-9592(98)00112-5

IARC (2012) *Chromium (VI) Compounds*, IARC Monographs on the Evaluation of Carcinogenic Risks to Humans, Vol. 100C. Lyon: International Agency for Research on Cancer. Available at: https://publications.iarc.fr/122

Ioannidou, O. and Zabaniotou, A. (2007) 'Agricultural residues as precursors for activated carbon production, A review', *Renewable and Sustainable Energy Reviews*, 11(9), pp. 1966-2005. doi: https://doi.org/10.1016/j.rser.2006.03.013

Jiao, X. *et al.* (2020) 'Recyclable superhydrophobic, antimoisture-activated carbon pellets for air and water purification', *ACS Applied Materials & Interfaces*, 12(22), pp. 25345-25352. doi: 10.1021/acsami.0c06274

Kano, F. *et al.* (2000) 'Fractal model for adsorption on activated carbon surfaces: Langmuir and Freundlich adsorption', *Surface Science*, 467(1-3), pp. 131-138. doi: 10.1016/S0039-6028(00)00730-5

Kumar, K.V. and Sivanesan, S. (2006) 'Equilibrium data, isotherm parameters and process design for partial and complete isotherm of methylene blue onto activated carbon', *Journal of Hazardous Materials*, 134(1-3), pp. 237-244. doi: 10.1016/j.jhazmat.2005.11.002

Lin, J. and Wang, L. (2009) 'Comparison between linear and non-linear forms of pseudo-first-order and pseudo-second-order adsorption kinetic models', *Frontiers of Environmental Science & Engineering in China*, 3(3), pp. 320-324. doi: https://doi.org/10.1007/s11783-009-0030-7

Lua, A.C. and Yang, T. (2004) 'Effects of activation temperature on the textural and chemical properties of activated carbon prepared from pistachio-nut shells', *Journal of Colloid and Interface Science*, 274(2), pp. 594-601. doi: https://doi.org/10.1016/j.jcis.2003.10.013

Luo, Y. *et al*. (2023) 'Hydrochar effectively removes aqueous Cr(VI) through synergistic adsorption and photoreduction', *Separation and Purification Technology*, 317, p. 123926. doi: https://doi.org/10.1016/j.seppur.2023.123926

Marsh, H. and Rodríguez-Reinoso, F. (2006) 'Activated Carbon', *Oxford: Elsevier*.

Mohan, D. *et al.* (2006) 'Activated carbons and low cost adsorbents for remediation of tri- and hexavalent chromium', *Journal of Hazardous Materials*, 137(2), pp. 762-811. doi: https://doi.org/10.1016/j.jhazmat.2006.06.060

Nasr, A.I. (2023) 'Conversion of chromium shaving waste into activated carbon', *Textile & Leather Review*, 6, pp .343-359. doi: 10.31881/TLR.2023.079

Oktavianty, H. and Anggoro, D.D. (2024) 'Adsorption kinetics of activated carbon from oil palm fronds', *E3S Web of Conferences*, 503, p. 09001. doi: https://doi.org/10.1051/e3sconf/202450309001

Valentín-Reyes, J. *et al.* 2019 'Adsorption mechanisms of hexavalent chromium from aqueous solutions on modified activated carbons', *Journal of Environmental Management*, 236, 2019, pp. 815-822. doi: https://doi.org/10.1016/j.jenvman.2019.02.014.

Burakov, A.E. *et al*. (2018) 'Adsorption of heavy metals on conventional and nanostructured materials for wastewater treatment purposes: A review', *Ecotoxicology and environmental safety*, *148*, pp. 702-712. doi: https://doi.org/10.1016/j.ecoenv.2017.11.034

Pina, A.C. *et al.* (2018) 'Supercapacitor electrode based on activated carbon wool felt', *C-Journal of Carbon Research*, 4(2), p. 24. doi: https://doi.org/10.3390/c4020024

Rodríguez, N.H., Martínez-Ramírez, S. and Blanco-Varela, M.T. (2016) 'Activated carbon as an alternative fuel: Effect of carbon ash on cement clinkerization', *Journal of Cleaner Production*, 119, pp. 50-58. doi: https://doi.org/10.1016/j.jclepro.2016.01.093

Rodríguez-Reinoso, F. (1998) 'The role of carbon materials in heterogeneous catalysis', *Carbon*, 36(3), pp. 159-175. doi: https://doi.org/10.1016/S0008-6223(97)00173-5

Rodríguez-Reinoso, F. *et al.* (1985) 'A comparison of the porous texture of two CO_2-activated botanic materials', *Carbon*, 23(1), pp. 19-24. doi: https://doi.org/10.1016/0008-6223(85)90191-5

Rodríguez-Reinoso, F. *et al.* (1987) 'A standard adsorption isotherm for activated carbons', *Journal of Physical Chemistry*, 91(3), pp. 515-516. doi: https://doi.org/10.1021/j100287a006

Shavandi, A. *et al.* (2017) 'Keratin: Dissolution, extraction and biomedical application', *Biomaterials Science*, 5(9), pp. 1699-1735. doi: https://doi.org/10.1039/C7BM00411G

Szczęśniak, B. *et al.* (2020) 'Mechanochemical synthesis of highly porous materials', *Materials Horizons*, 7(6), pp. 1457-1473. doi: https://doi.org/10.1039/D0MH00081G

Tang, W. *et al.* (2021) 'Influence of cuticle layers and activators on tubular activated carbon from wool waste', *Powder Technology*, 392, pp. 38-46. doi: https://doi.org/10.1016/j.powtec.2021.06.045

The Woolmark Company (2018) *The Wool Supply Chain: Environmental Considerations in Wool Processing*.

Tuinstra, F. and Koenig, J.L. (1970) 'Raman spectrum of graphite', *Journal of Chemical Physics*, 53(3), pp. 1126-1130. doi: https://doi.org/10.1063/1.1674108

Wang, L. *et al.* (2010) 'Adsorption of Pb (II) on activated carbon prepared from Polygonum orientale Linn.: kinetics, isotherms, pH, and ionic strength studies', *Bioresource technology*, *101*(15), pp. 5808-5814. doi: https://doi.org/10.1016/j.biortech.2010.02.099

Zhang, B. *et al.* (2025) 'Two-Step Hydrothermal Reaction Enhances Removal of Cr(VI) from Wastewater Using Nitrogen-Doped Starch-Based Hydrothermal Carbon', *Sustainability*, *17*, p. 4982. doi: https://doi.org/10.3390/su17114982